PHYSICAL REVIEW A VOLUME 51, NUMBER 6 JUNE 1995

Dynamical analysis of Brillouin fiber lasers: An experimental approach

S. Randoux, V. Lecoeuche, B. Ségard, and J. Zemmouri
Laboratoire de Spectroscopie Hertzienne, Université de Lille 1, 59655 Villeneuve d'Ascq, France
(Received 4 August 1994; revised manuscript received 7 December 1994)

We study experimentally and numerically the influence of the fiber length on the stability of Brillouin lasers in both ring cavity and Fabry-Pérot configurations. For short enough fibers, experiments and numerical simulations show that the Brillouin emission is stable for any input pump power. This behavior, in contrast with that previously observed on long fibers, is interpreted within the framework of a modal analysis. Further experiments, involving a sweeping of pump frequency, emphasize the role of the frequency detunings, which was generally overlooked.

PACS number(s): 42.65.Es, 42.50.Ne, 42.81.−i

In the field of nonlinear dynamics, the study of stimulated Brillouin scattering (SBS) in optical fibers has recently attracted a great deal of interest [1–4]. Feedback from the fiber ends is known to introduce instabilities leading to periodic and quasiperiodic behaviors [1,4,5]. In the ring cavity configuration, the SBS emission may exhibit solitonic regimes [6]. One important result, common to the previous works, is the absence of stable laser emission beyond the threshold [4–9]. This behavior can be understood if one considers that these studies are performed with fiber lengths on the order of a few hundred meters. Such lengths lead to an important single-pass gain and then obviously contribute to a decrease in the lasing threshold when the fiber is enclosed in a resonator. The free spectral range (FSR) of this cavity (a few megahertz) is then much narrower than the width of the Brillouin gain curve which is about 100 MHz at 514 nm, the pumping wavelength commonly used. Thus numerous cavity modes lying near the center of the gain curve have almost identical gains. A strong mode competition then manifests itself just above the threshold, leading to the observed unstable regimes.

The aim of this paper is to analyze the influence of the fiber length on the SBS laser dynamics and to quantify the role of the cavity modes in the establishment of the instabilities. In accordance with a modal analysis, numerical simulations show evidence that the instabilities only occur for long enough fibers and, contrary to the previous works, not necessarily just above the lasing threshold. The results are successfully compared with experiments involving a sweeping of the pump power. Further experiments, performed by sweeping the pump frequency, point out the effect of the frequency detuning of the Stokes wave upon the laser behavior.

Our numerical study enters into the framework of the usual coherent three-wave SBS model [7,9] characterized by the dimensionless equations

$$\partial_t E(z,t)+\partial_z E(z,t)=-gB(z,t)E_s(z,t)-\beta E(z,t),$$

$$\partial_t E_s(z,t)-\partial_z E_s(z,t)=gB^*(z,t)E(z,t)-\beta E_s(z,t), \quad (1)$$

$$(1/\beta_a)\partial_t B(z,t)+B(z,t)=E(z,t)E_s^*(z,t),$$

where $E(z,t)$, $E_s(z,t)$ are, respectively, the pump and Stokes complex field amplitudes, normalized to the maximum amplitude of the input pump field E_0. $B(z,t)$ is proportional to the acoustic wave amplitude. g is the SBS gain parameter, β is the attenuation coefficient of the optical fields, $\beta_a=\pi\Delta\nu_B nL/c$ is the acoustic wave damping coefficient, L the fiber length, c the velocity of light, and n the fiber refractive index. $\Delta\nu_B$ is the Brillouin gain bandwidth, estimated to 60 MHz (full width at half maximum) at a working wavelength of 800 nm [10]. This model is completed by boundary conditions, which in the case of a ring cavity are

$$E_s(L,t)=\rho E_s(0,t)\exp(i\psi_s),$$
$$E(0,t)=\rho E(L,t)\exp(i\psi_p)+\mu. \quad (2)$$

ψ_s (ψ_p) is the accumulated phase difference per round trip due to a possible mismatch between a cavity resonance and the Stokes (pump) wave frequency. ρ is the reinjection rate and μ is a dimensionless pumping parameter.

The stationary solutions of Eqs. (1) and (2) can be obtained by canceling the time derivative of the moduli and assuming the time derivative of the phases to be constant in order to take into account possible frequency shifts [11], but usually all the time derivatives are set to zero. This restrictive assumption leads to a set of coupled equations for the moduli, all phases being independent of the spatial variable z [12]. This imposes a phase continuity at $z=0$ and L, and the model then implicitly includes the resonance condition $\psi_p=\psi_s=0$ usually assumed in previous works [4–9]; in particular, those evidencing instabilities just beyond the lasing threshold. A direct comparison with those results requires us to perform our simulations in this fully resonant condition. In spite of this limiting assumption, our simulations allow us to analyze the role of the fiber length on the laser dynamics, which was overlooked in most of the previous studies, where the system behavior is described by a "gain factor" proportional to LE_0^2 [8,9].

The numerical phase diagrams corresponding to the ring and to the Fabry-Pérot lasers are respectively shown in Figs. 1(a) and 1(b). In the first case, the value of the feedback parameter is estimated from our experiments ($\rho=0.36$). In the case of the Fabry-Pérot laser (i.e., a finite-length medium

 © 1995 The American Physical Society

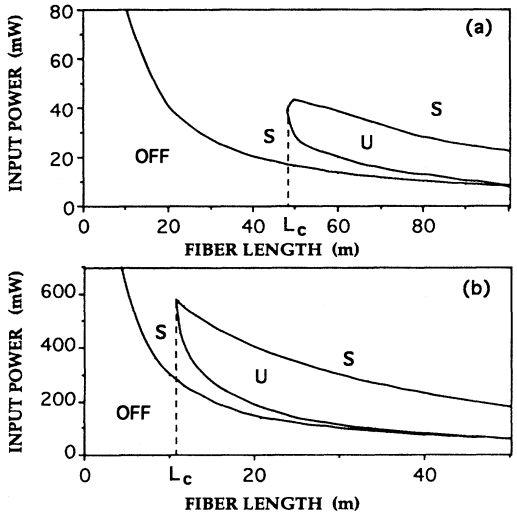

FIG. 1. Numerical phase diagram in the case of: (a) ring cavity; (b) Fabry-Pérot cavity. S and U respectively indicate the stable and the unstable domains.

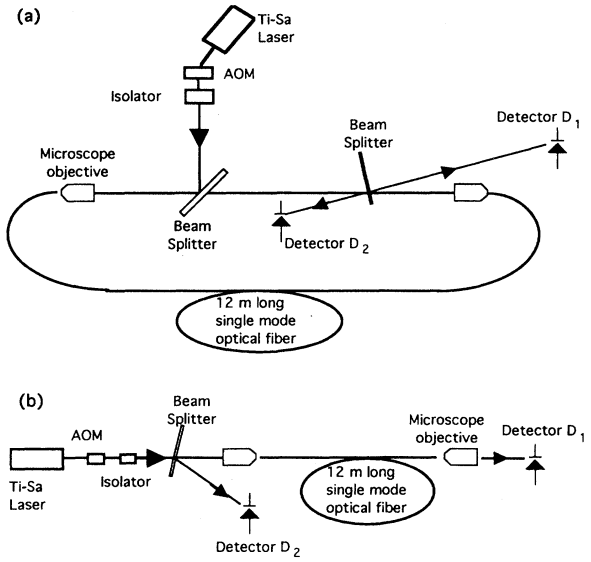

FIG. 2. Schematic setup of the experimental arrangement: (a) ring cavity; (b) Fabry-Pérot cavity.

with reflective boundaries), the set of equations (1) is completed by a similar one (with $\partial_z \rightarrow -\partial_z$) for the reflected waves; the system dynamics is then described by two independent sets of three equations. The backward and forward propagating pump (SBS) waves are coupled by boundary conditions corresponding to Fresnel glass-air reflections.

As shown in the two numerical diagrams, the Fabry-Pérot laser and the ring laser globally exhibit the same dynamics. Depending on the fiber length, three distinct dynamical behaviors can be distinguished:

(i) For fiber lengths lower than a critical value L_c, the SBS emission remains stable for any input pump power. This can be interpreted within the framework of a modal analysis. In this case, the cavity FSR is comparable with the width of the Brillouin gain curve, and only a few modes can experience gain. Near the threshold, only the mode that coincides with the center of the gain curve has sufficient gain to overcome the resonator losses and can oscillate. Since the Brillouin curve is homogeneously broadened, the laser always remains monomode as the input power increases [13].

(ii) For long enough fibers, the SBS emission is unstable just beyond the threshold. In this case, the resonator FSR is so small that many of the modes close to the center of the gain curve nearly experience the same gain and can oscillate simultaneously near the threshold. This leads to the unstable behaviors observed in previous works [4–9].

(iii) The transition between the dynamical behaviors observed in the two previous cases (short and long fibers) occurs inside a range of intermediate lengths. The SBS emission, stable and therefore monomode near the threshold, becomes unstable for sufficiently high pumping levels.

Note that, for any fiber length, the "Brillouin mirror" regime may be reached by sufficiently increasing the pumping level. The modal analysis, previously introduced in order to describe the laser's behavior near the threshold, also allows us to explain the difference between the values of the critical lengths obtained for the ring laser (48 m) and for the Fabry-Pérot laser (11 m). For a given fiber length, the Fabry-Pérot FSR is half that of the ring cavity. Thus, if the two resonators had the same quality factor, the critical length characterizing the Fabry-Pérot would be half that of the ring laser (i.e., 24 m). However, in our numerical simulations, the Fabry-Pérot quality factor is much lower than that of the ring cavity. The strong overlapping between modes then favors their competition and the critical length is reduced (<24 m).

In our experiments, we have chosen a 12-m-long monomode fiber (polarization maintaining) in order to investigate the experimentally unexplored phase diagram region and to check our numerical predictions. This length is indeed smaller than L_c in the ring cavity case and slightly larger than L_c in the Fabry-Pérot configuration (Fig. 1). The experimental setup of the ring cavity is schematically shown in Fig. 2(a). The cw emission of a single-mode titanium:sapphire laser operating at 800 nm is used as a pump source. This laser is characterized by a 500-kHz linewidth, and its frequency can be linearly swept over a range adjustable from 10 MHz to 30 GHz. It is optically isolated from the ring cavity by a Faraday isolator, and the incident pump power is controlled by an acousto-optic modulator (AOM). Input and output fiber coupling are achieved through 20× microscope objectives; the maximum power injected into the fiber is then about 100 mW. A low reflectivity beam splitter, inserted inside the cavity, respectively reflects the pump copropagating and counterpropagating beams towards two silicium photodiodes D_1 and D_2, which have a 200-MHz frequency bandwidth. Finally, these are connected to a 125-MHz oscilloscope. The Fabry-Pérot experiments, which require a much higher coupled power, are performed with the experimental setup displayed in Fig. 2(b). The first-order Stokes emission appears for an injected power of about 270 mW. An external interferometer has been used to check that higher-order Stokes components do not appear.

Figure 3 shows the Stokes (detector D_2) and transmitted pump (detector D_1) signals typically observed in the case of the ring laser, when the input pump power is linearly swept.

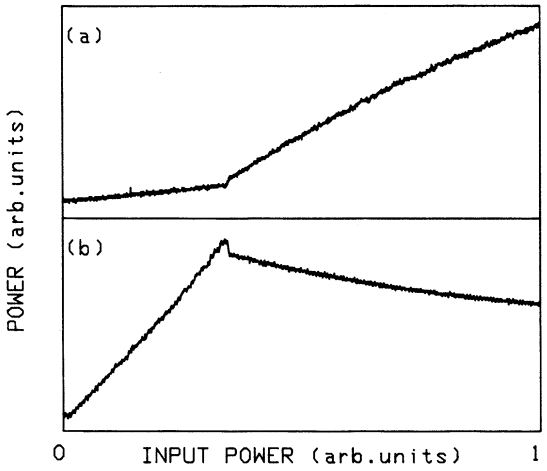

FIG. 3. Ring cavity. Experimental signals recorded while slowly sweeping the input pump power. (a) Stokes power; (b) transmitted pump power.

The sweeping rate is sufficiently slow (100 Hz) to avoid dynamical effects on the location of the bifurcation points. The optical length of the cavity is not externally stabilized. Thus the resonance conditions, imposed in the numerical simulations, are not fulfilled in the experiments. In particular, the peak of the Brillouin gain curve does not necessarily coincide with one cavity mode. However, the SBS emission is stable beyond the lasing threshold. This remains compatible with our modal analysis; the homogeneously broadened Brillouin line indeed restricts the oscillation to the mode nearest the center of the gain curve.

In the case of the 12-m-long Fabry-Pérot laser, Fig. 4 shows a typical result obtained by slowly sweeping the input pump power. Stable SBS emission occurs just beyond the lasing threshold, and periodic instabilities appear, via a Hopf bifurcation, for higher input powers. The frequency of these instabilities is equal to the Fabry-Pérot FSR (8.6 MHz) and is characteristic of a mode beating.

In order to quantify the role of the frequency detuning between the center of the gain curve (ν_s) and the nearest

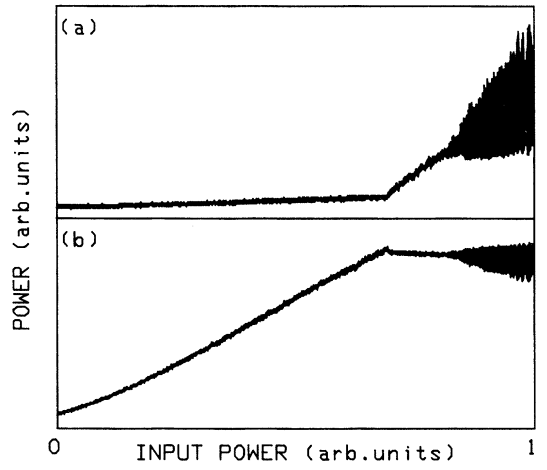

FIG. 4. Fabry-Pérot cavity. Same as Fig. 3: (a) Stokes power; (b) transmitted pump power.

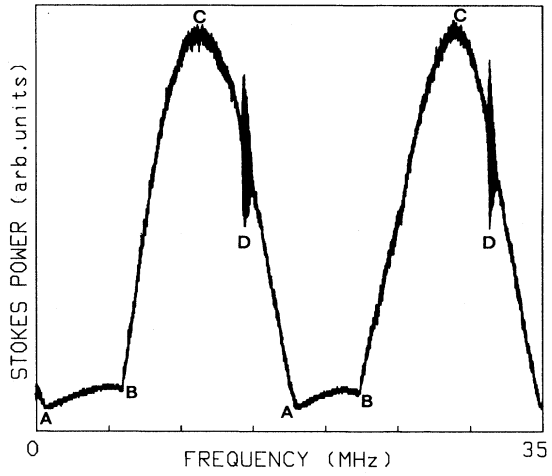

FIG. 5. Ring cavity. Experimental Stokes signal recorded while slowly sweeping the pump laser frequency. The swept range corresponds to about twice the cavity FSR.

cavity mode (ν_c), we have performed a sweeping of the frequency of the pump laser at constant power. Let us emphasize that this frequency sweeping entails two main effects: (i) a displacement of the Brillouin gain curve and then a modification of the frequency detuning $\nu_s - \nu_c$; (ii) a periodic change in the intracavity pump field, which leads to a change in the intracavity Stokes field. This latter effect is responsible for the periodic modulation of the Stokes power evidenced in Fig. 5. This recording was obtained for the ring laser by slowly sweeping the frequency of the pump laser over two cavity FSR's. Within the interval A-B, the pump laser frequency is halfway between two resonances of the passive cavity (antiresonant configuration), and the intracavity pump field is too low to initiate the SBS emission. Sweeping the laser frequency from point B to point C leads to an increase in the intracavity pump field, which becomes sufficiently high to give rise to the Stokes wave. From the

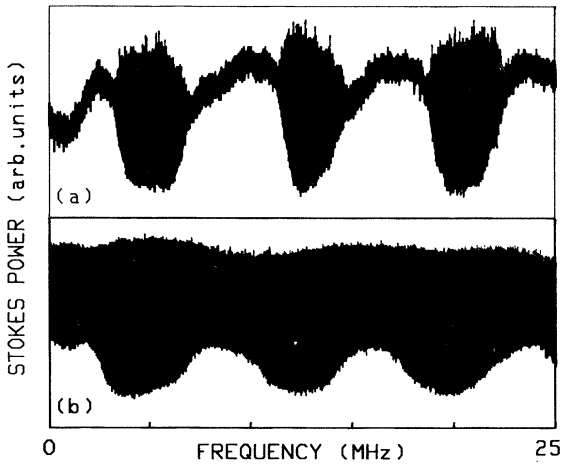

FIG. 6. Fabry-Pérot cavity. Experimental Stokes signal recorded while slowly sweeping the pump laser frequency at (a) low input power and (b) high input power. The swept range corresponds to about three cavity FSR's.

lasing threshold (point B), the SBS emission is stable and then involves the cavity mode nearest the peak of the Brillouin gain curve. The power of the Stokes field reaches its maximum (point C) when the intracavity pump field is maximum; the pump wave is then resonant with one cavity mode ($\psi_p = 0$). A further increase in the frequency of the pump leads to a deviation from this resonance condition, and both the pump and Stokes powers decrease (interval C-A). Apart from this modulation of the field powers, the sweeping of the pump frequency entails a sweep of the frequency detuning $\nu_s - \nu_c$. Each time this latter is equal to half the cavity FSR, the center of the Brillouin gain curve is in antiresonant configuration and two modes then experience the same gain. Thus they can oscillate simultaneously, then giving rise to the mode beating observed around the points D. In fact, the SBS emission is always stable and single-mode, except in regions D where a mode hop occurs. Due to the Brillouin shift (20 GHz), the cavity antiresonant configuration observed at the Stokes frequency departs from that observed at the pump frequency. The position of the mode hops then depends on the relative values of the cavity FSR and the Brillouin shift, and they can be located at any point inside an interval A-A. For higher pump powers, the SBS laser always operates above the lasing threshold and the region A-B is not observed.

In the case of the Fabry-Pérot laser, Fig. 6(a) shows the evolution of the SBS output when the frequency of the pump laser is slowly swept over about three FSR. Because of the low-quality factor of the cavity, the modulation depth of the pump and Stokes powers is much lower than for the ring laser. On the recording, Fig. 6(a), the pump power is adjusted above threshold in the stable domain of Fig. 1(b). As the mode competition is favored, the ranges of instabilities associated with the mode hops are enlarged, but the laser remains stable in wide domains around the resonance between one cavity mode and the peak of Brillouin line. For higher pumping levels, inside the instability domain of Fig. 1(b), the laser is unstable for any pump frequency [Fig. 6(b)].

In summary, we have evidenced the existence of a critical length under which SBS lasers remain stable for any input pump power. Near the lasing threshold, the SBS laser behavior is interpreted within the framework of a simple modal analysis. The effect of a cavity-Stokes frequency mismatch does not affect significantly the stability of the emission.

[1] R. G. Harrison, J. S. Uppal, A. Johnstone, and J. V. Moloney, Phys. Rev. Lett. **65**, 167 (1990).

[2] C. C. Chow and A. Bers, Phys. Rev. A **47**, 5144 (1993).

[3] A. L. Gaeta and R. W. Boyd, Phys. Rev. A **44**, 3205 (1991).

[4] M. Dämming, G. Zinner, F. Mitschke, and H. Welling, Phys. Rev. A **48**, 3301 (1993).

[5] R. G. Harrison, P. M. Ripley, and W. Lu, Phys. Rev. A **49**, R24 (1994).

[6] E. Picholle, C. Montes, C. Leycuras, O. Legrand, and J. Botineau, Phys. Rev. Lett. **66**, 1454 (1991).

[7] J. Botineau, C. Leycuras, C. Montes, and E. Picholle, J. Opt. Soc. Am. B **6**, 300 (1989).

[8] I. Bar-Joseph, A. A. Friesem, E. Lichtman, and R. G. Waarts, J. Opt. Soc. Am. B **2**, 1606 (1985).

[9] C. Montes, A. Mamhoud, and E. Picholle, Phys. Rev. A **49**, 1344 (1994).

[10] G. P. Agrawal, *Nonlinear Fiber Optics* (Academic, Boston, 1989).

[11] J. Botineau, C. Leycuras, C. Montes, and E. Picholle, Ann. Télécommun. **49**, 479 (1994).

[12] J. Botineau, C. Leycruas, C. Montes, and E. Picholle, Opt. Commun. **109**, 126 (1994).

[13] See, for example, O. Svelto, *Principles of Lasers*, 3rd ed. (Plenum, New York, 1989).